International Journal of Refrigeration 179 (2025) 295–303

Contents lists available at ScienceDirect

International Journal of Refrigeration

journal homepage: www.elsevier.com/locate/ijrefrig

INSTITUT INTERNATIONAL DU FROID
INTERNATIONAL INSTITUTE OF REFRIGERATION

Experimental study about frost formation and growth in the evaporator of an air-to-water heat pump

David Alarcón-Gallén [a], Javier Marchante-Avellaneda [a], Abdelrahman H. Hassan [a,b,*], Emilio Navarro-Peris [a]

[a] Instituto Universitario de Investigación en Ingeniería Energética (IIE), Universitat Politècnica de València (UPV), Camino de Vera S/N 46022, Valencia, Spain
[b] Mechanical Power Engineering Department, Faculty of Engineering, Zagazig University, Zagazig 44519, Egypt

ARTICLE INFO

Keywords:
Frost
Heat pump
Finned-tube heat exchanger
Pressure drop

ABSTRACT

Frost formation in the evaporator of air-to-water heat pumps (AWHPs) is one of the most crucial aspects that affect the efficiency of these systems. This paper analyzes the frost formation and growth in a finned-tube evaporator to monitor the degradation of a commercial heat pump's performance. The analysis includes the characterization of the various frost formation processes that may occur in real operating conditions, as well as a detailed examination of the water vapor sublimation process as a function of evaporation temperature and relative humidity. The results are presented in terms of the air-side pressure drop, evaporation temperature evolution, and the amount of condensed water recovered. From these results, key factors in the evolution of this process, like the frost structure, are critical in the system performance degradation, and parameters like air-side pressure drop are not enough to determine the optimum time for initiating the defrost process.

1. Introduction

Heat pump systems are a key technology for the decarbonization of the building sector, and among them, air-to-water heat pumps (AWHPs) are seen as the clear alternative to substitute gas boilers, which are the most common systems used in the European Union (EU) to satisfy the heating demand in buildings (European Commission, n.d).

Nevertheless, when these systems work at low operating temperatures, frost formation on the finned-tube heat exchanger's (FTHX) surface substantially degrades system efficiency by restricting airflow and increasing thermal resistance. As the frost layer develops, periodic defrosting is required to restore optimal thermal performance.

Because of its significance, frost formation, growth, properties, and morphology have been widely analyzed and reviewed in different studies (Song and Dang, 2018; Zhang et al., 2022).

Many works focus on the individual performance of a simple FTHX (one row and/or one refrigerant circuit) under frost conditions. These are usually installed in a controlled wind tunnel using a single-phase refrigerant, i.e., water-ethylene (Hwang and Cho, 2014; Zhang et al., 2019).

Nevertheless, there are few studies in the literature about the most specific problem of frost formation and growth in a FTHX installed within an AWHP, and most of them are focused on proposing techniques to reduce frost formation or to optimize the defrost time. A review of some of those works can be found in Song et al. (2018). In that line, some works can be cited, like Guo et al. (2008) who characterize the frost growth in a heat exchanger and the degradation of the heat pump performance. The study of the effect of the airflow rate on the frost impact on AWHPs (Liang et al., 2024), or the frost growth characterization in a FTHX coupled with a fan, where the relative importance of different operating parameters is also evaluated, showing that the frost clogging effect has more impact on system degradation compared to the change in heat transfer coefficient (Da Silva et al., 2011).

Da Silva et al. (2017) also highlight the fact that the impact on the system efficiency depends not only on the amount of frost but also on other factors, such as how it is accumulated, the coating of the surface, or how the frost is formed. This fact motivated the analysis of the surface characteristics of the heat exchanger and how it affects the frost growth (Wang et al., 2015a), or others who have focused on developing a method or maps to characterize it, obtaining a quantitative or qualitative value on frost severity, and providing information about the frost formation process (Zhu et al., 2015).

The main application of these approaches has been oriented to evaluate the optimum defrost time depending on some additional

* Corresponding author.
E-mail address: ahassan@iie.upv.es (A.H. Hassan).

https://doi.org/10.1016/j.ijrefrig.2025.08.013
Received 21 May 2025; Received in revised form 26 July 2025; Accepted 10 August 2025
Available online 11 August 2025
0140-7007/© 2025 The Author(s). Published by Elsevier B.V. This is an open access article under the CC BY-NC-ND license (http://creativecommons.org/licenses/by-nc-nd/4.0/).

parameters, but unfortunately, it isn't easy to use these approaches to assess the heat exchanger design quantitatively.

The main problem in developing this kind of assessment is related to the fact that models available in the literature usually focus on only one type of frosting process, and they are also based on a limited amount of data to validate them. This paper analyzes the frosting phenomenon in a FTHX coupled with a fan and installed in a commercial AWHP. The main objectives of the article are:

- To characterize the different water frosting processes that can appear in a FTHX depending on the air conditions.
- To report the observed differences among them and the sources of variability.
- To supply a characterization of the frost formation and growth process in terms of AWHP's key parameters like the amount of water defrosted, the air-side pressure drop, and the evolution of evaporation temperature as a function of air conditions (humidity and temperature).

The analysis is divided into two parts. In the first one, based on the different frost formation processes, a characterization of the heat pump performance degradation has been made. In the second one, a wider experimental campaign for different air temperatures and relative humidities has been performed, focusing on the frost formation under sublimation and near-sublimation (condensation + frost conditions with vapor pressure near sublimation) conditions. From all the results obtained in the experimental campaigns, the different stages in the frost formation process have been determined, showing the most critical points of the process in such a way that design criteria can be obtained to increase the evaporator performance working under frost conditions. As mentioned before, the analysis has been made in a commercial AWHP, not an individual analysis of the FTHX. On the one hand, this fact will introduce additional variability to the process itself, but on the other hand, it will provide a more accurate representation of frost formation under real-world operating conditions.

2. Experimental campaign

2.1. Experimental setup

A modified commercial AWHP unit of 8 kW nominal capacity has been used for the test. The AWHP comprises a variable-speed twin-rotary compressor, a brazed plate heat exchanger (BPHX) with 30 plates, a FTHX with the characteristics shown in Table 1 and the circuit pattern shown in Fig. 1, an electronic expansion valve (EEV), a 4-way reversible valve, and an accumulator at the outlet of the evaporator. The expansion valve maintains the subcooling at a value of 5 K in all tests, and the heat pump operates with a superheat of 0 K at the evaporator outlet. This allows for avoiding refrigerant maldistribution in the evaporator and ensures a homogenous frost formation. Moreover, the configuration of the AWHP under study has a suction line accumulator (Fig. 2), instead of a liquid line, to optimize the subcooling, allowing better temperature matching between the refrigerant and water to enhance the COP.

Table 1
Main characteristics of the finned-tube heat exchanger.

Characteristics [unit]	Value
Tube spacing [mm]	25
Row spacing [mm]	21.65
Rows/Tubes per Row [-]	3/32
Fin spacing [mm]	2.2
Fin thickness [mm]	0.1
Finned length [m]	0.7
Number of Circuits [-]	8
Tube outer diameter/Tube thickness [mm]	7.2/0.43 (riffled type)
Coating & wettability [-]	Superhydrophilic (contact angle < 10°)

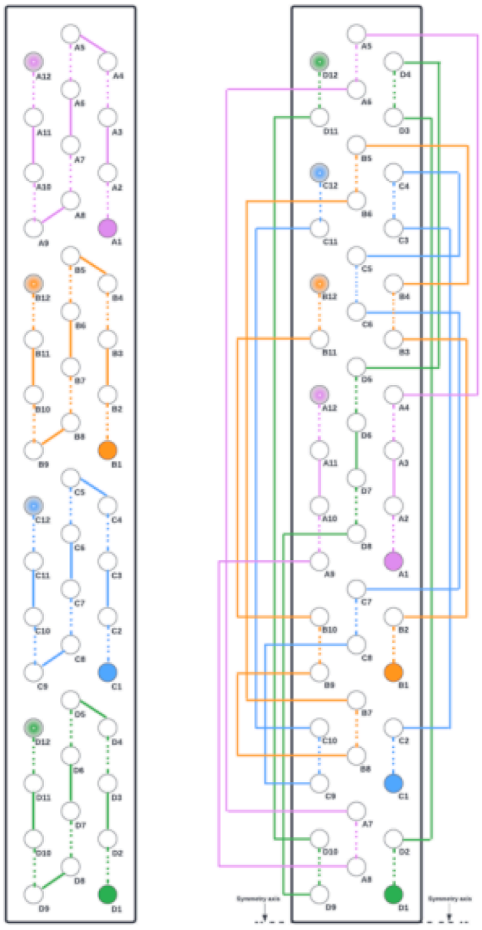

Fig. 1. Refrigerant circuit pattern of the evaporator used in this work (the pattern is symmetric, so only four circuits are shown in the Fig.).

The AWHP was instrumented according to the scheme shown in Fig. 2. It shows that temperature sensors were installed at the inlet and outlet of each component, pressure sensors were installed at the inlet and outlet of the compressor, a Coriolis mass flow meter was installed at the condenser outlet and on the secondary water circuit, and wattmeters were installed to measure the consumption of the fan and compressor. All these instrumentations were focused on monitoring the heat pump operating conditions. More specifically, to monitor the frost formation, a pitot tube was installed to measure the air pressure drop in the FTHX, and a digital camera was installed to record the frost growth in the frontal section and monitor the blockage of the free-flow area with time. The statistical software R (R Foundation for Statistical Computing, 2021) and an open-source video processing FFmpeg tool (FFmpeg Developers, 2016) have made it possible to program a simple script to analyze the frost formation process and perform a qualitative analysis. This methodology is described in Yoo et al. (2018). It consists of image analysis for each recorded video frame and classification of each image pixel into frost or non-frost conditions depending on its brightness level. The authors showed the simplicity and validity of this method, which allows a qualitative monitoring of frost growth evolution with time and other important frost formation mechanisms.

The script obtains several frames of the recorded videos and analyzes the brightness of each pixel to estimate the blocking ratio BR (ratio of frost area to the total inlet area) for the entire test duration. This blocking ratio is calculated as shown in Equation 1:

$$BR = \frac{Number\ of\ pixels\ at\ frosting\ stage}{Total\ number\ of\ pixels} \quad (1)$$

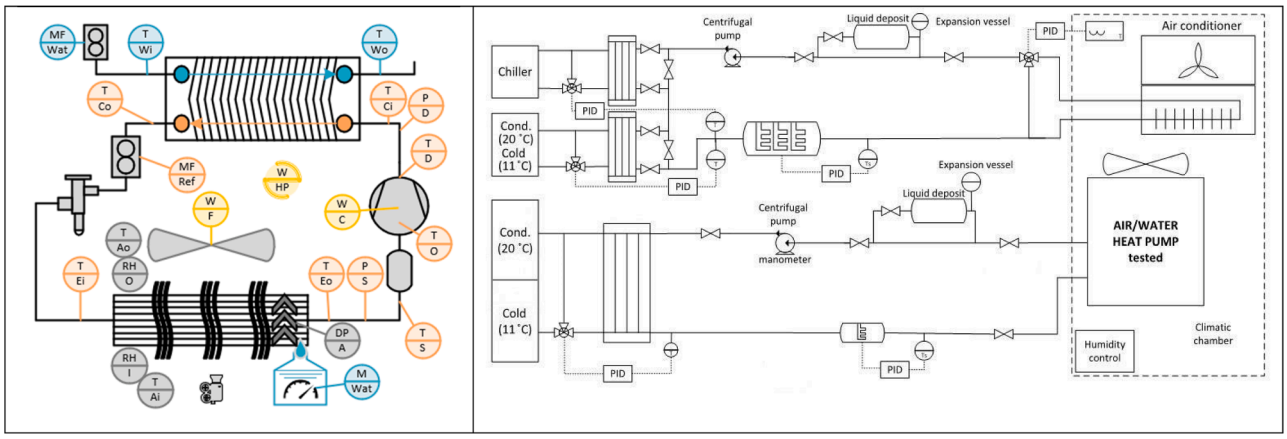

Fig. 2. Scheme of the instrumentation in the heat pump unit (Left), and climatic chamber used to test the heat pump (Right).

Moreover, the total frost mass, during one frost formation cycle, is measured with a scale. To do so, a tray at the bottom of the evaporator was utilized to collect all the condensed water after the defrosting process. It should be noted that part of the condensed water remains stuck to the evaporator surface after defrosting. To mitigate this, the evaporator was blown out after each test to recover and drain the water more effectively.

The AWHP's control unit monitors the heating capacity, determines an initial capacity, and calculates its degradation with time in each measurement; when the capacity is degraded by 15 % compared to the initial value, it determines that the defrost process must be started. From the authors' point of view, that threshold could serve as a practical and qualitative measure of performance degradation to justify the initiation of the defrost process. Nevertheless, this value is not a critical factor in the current study or the proposed methodology, as the presented work focuses on the analysis of frost growth and how it affects the system's performance. In fact, it could be adjusted to other values without major changes in the presented results or findings.

The AWHP has been installed inside a climatic chamber capable of controlling air temperature and humidity. The climatic chamber can control the air temperature conditions between -25 °C and 50 °C and the relative humidity (RH) between 20 % and 90 %. Regarding the water side, the heat pump was connected to a water loop, which was able to control the water temperature between 7 °C and 80 °C. Table 2 shows the measured variables, the types of sensors used in the measurements, and uncertainties.

Table 2
Measured variables, characteristics of the sensors, and uncertainties (U95 is 95 % uncertainty confidence).

Variable	Equipment	U95	Comments
T	Thermocouple Type T C1	±0.8 (°C)	Inlet and outlet temperatures of refrigerant for main components (surface measurement).
T	PT100	±0.12 (°C)	Water and air at the inlet and outlet of the unit.
P	Pressure Transducer	±0.06 (*bar*)±0.27 (°C)	Suction and discharge pressures. Used for saturation temperature calculation.
ΔP	Pressure Transducer	±3.7 (*Pa*)	Air-side pressure drop.
W	A2000	±0.0144 (*kW*)	Energy consumption of the compressor, fan, and heat pump.
RH	-	±2.8 (°C)	Relative humidity of air at the inlet and outlet of the FTHX.
Scale	CB12K1N	±3 (*g*)	Mass of the condensed/ defrosted water.

2.2. Test matrix

The frost formation mechanism in a heat exchanger can be classified according to the water phase change process into two mechanisms. In the first one, the water condenses first on the surface of the FTHX, then it freezes. In the second one, the vapor is sublimated directly to frost over the FTHX's surface. More details about this classification will be discussed later (Section 3.1. Characterization of the frost formation mechanism). During all the tests, the compressor and fan speed were kept constant.

Based on that, the experimental campaign was divided into the following two parts. The first part analyzes the frost production mechanism under the following conditions:

- Relative humidity [%]: 90.
- Air dry-bulb temperature [°C]: 10, 7, 2, -3, -7.

In these conditions, the total frost mass is measured with a scale, and the frost formation is recorded with a video camera. The videos recorded allow us to obtain the start/final time of frost formation and the blocking ratio in the FTHX.

The second part focuses on the characterization of the frost formation process by sublimation. Later, and for the points in which the frost was formed by sublimation, a more detailed study will be performed for a wider set of air temperatures and relative humidities.

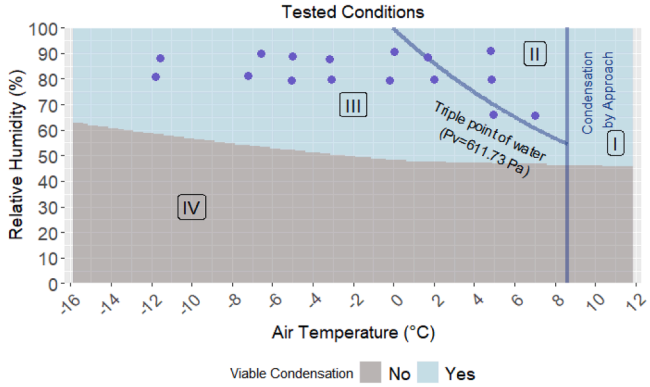

Fig. 3. Test matrix of the current study (the diagram is divided into four zones: I-condensation, II-condensation + frosting, III-sublimation, IV-dry).

Fig. 3 shows the test matrix of 16 working conditions that were experimentally tested and the frost/condensation mechanism of each point. Very cold and low-humidity conditions were discarded as the frost formation rate was very low. Fig. 3 defines four zones. Zone I refers to the dehumidification/condensation (no frost), Zone II refers to the condensation that could, with time, freeze due to sub-zero surface temperature, Zone III represents the sublimation frosting zone (without condensation), and Zone IV refers to totally dry conditions (no condensation or frost). To distinguish between the different zones, two boundaries are defined. The first one is the partial vapor pressure that distinguishes between condensation + frosting (II) and sublimation frosting (III) zones based on the psychometric air properties (triple point of water as limit). The second one is related to the temperature difference between FTHX's surface and the surrounding air. Zone I is defined by the approach temperature (frost does not form if the surface temperature is above 0°C), and zone IV is defined by the dew point-approach temperature (neither condensation nor frosting occurs if the air dew point temperature is lower than the surface temperature).

2.3. General observations during the tests

- Instabilities or oscillating behavior in the evaporation temperature have been observed when their values are low. The control performed by the EEV introduces these instabilities.
- It is important to note that measuring the pressure drop under frost conditions presents significant challenges, as frost accumulation can obstruct sensors and measurement devices, introducing deviations in the real pressure drop measurements. This fact could be solved in the laboratory test, incorporating small heaters in the sensors, but it is challenging to use these kinds of measurements in field operation.
- It should be noted that a comparison of the system performance with and without frost formation cannot be made very precisely, since the humidity in the ambient air determines the latent heat energy available in the air and, depending on this, the source conditions change.
- Repeatability of the test can be challenging in real conditions, as some kind of hysteresis could be present in the frost formation process in such a way that, depending on the previous condition, certain air conditions could produce or not produce frost (due to the hysteresis of the EEV, the evaporation temperature could vary slightly, and this could affect the frost formation process).
- Water retention on the FTHX after the defrost cycle is an important factor to consider when frost formation is analyzed for a heat pump working in real conditions.

3. Results and discussion

To understand the effect of frost formation on the performance of AWHPs, many parameters and indicators should be addressed and evaluated. This includes the amount of defrosted water, the heating period duration, the airflow reduction with time, and general performance indicators such as heating capacity and coefficient of performance (COP).

3.1. Characterization of the frost formation mechanism

In this first experimental campaign, two types of frost formation processes have been identified, and the tests can be divided into two types:

- Tests with positive temperatures and high moisture content in the air (moderate climate temperatures with high relative humidity values).
- Tests with negative temperatures where the absolute moisture content in the air is low (cold climate temperature and low relative humidity values).

Fig. 4 shows the process for the two extreme points tested, with an air dry-bulb temperature of 10 and -7 °C, and fixed RH of 90 %.

We can observe how, for the air conditions of 10 °C and RH 90 %, we obtain a non-homogeneous frost generation at the inlet surface of the FTHX. On the other hand, for the air conditions of -7 °C and RH 90 %, we obtain a more homogeneous frost generation. This behavior is directly related to the different mechanisms of frost formation. The frost formation process presents two typologies depending on the air conditions (Tang et al., 2021). Fig. 5 shows the three-phase diagram of water vapor in the air.

Consider two air streams, "C" and "S", which are at the same dry-bulb air temperature (C1 and S1), but the water content is different. Thus, the partial vapor pressure p_v, in Pa: for C is $P_v > P_{TP}$ and for the S is $P_v < P_{TP}$, where P_{TP} is the vapor pressure at the triple point (TP) of water. Both streams are cooled as they go through an evaporator.

Regarding the S stream, as the air is cooled, it reaches 0°C at S3, while it is not yet saturated. As it cools further, it reaches S4; in these conditions, the water vapor content is sublimated to frost. While the air is cooled down following the saturation line, during this process, more water sublimates to frost.

Regarding the C stream, it reaches saturated conditions at C2, so water vapor content in the air starts to condense. Condensed water is cooled until C3, when it starts to freeze, turning into ice. While the air flow is cooled following the saturation line, condensing more water during this process till reaching the TP, from this point, the remaining water vapor in the air begins to sublimate.

When this air flows through a heat exchanger (evaporator), its temperature decreases, so the relative humidity increases, leading to saturation conditions. As can be seen, the C stream reaches the saturation condition above 0°C, at C2, while the S stream reaches it below 0°C, at S4. Based on this, two typologies of frost formation could be identified: Condensation + Frost (C+F) and Sublimation (S).

Once the frost formation mechanisms have been identified, the analysis starts with the calculation of the blockage ratio (BR), or the percentage of free-flow area that is blocked by frost. Fig. 6 shows the results obtained for each of the five different inlet air conditions. The Fig. shows that for high air temperatures, the defrost is initiated later but at lower values of the BR parameter, showing that the degradation in the capacity is not always directly related to the BR. Therefore, a visual analysis may not be accurate enough to determine when a defrost should be initiated.

Table 3 summarizes the most relevant variables in the analysis of frost formation and growth. Each experimental test is evaluated within a complete cycle, which includes two stages. The heating stage (the AWHP works in its normal mode, and during this, the frost starts to accumulate on the evaporator), and the defrost stage (the cycle is inverted using the 4-way valve to allow the defrosting process and eliminate the frost generated on the evaporator surface). Table 3 includes the following results:

- The degradation of the heating capacity.
- The average value for the partial pressure of water vapor in the inlet air during the heating stage. This value allows us to identify the frost mechanism considering the partial pressure of water vapor in the triple-point as 611.657 Pa.
- The maximum BR before executing the defrost cycle. It is obtained from visual analysis and Equation 1.

Equation 2 shows how to calculate the heating capacity degradation (HCD) parameter:

$$HCD(\%) = \left(1 - \frac{\dot{Q}_{t=defrost}}{\dot{Q}_{t=0}}\right) \times 100 \quad (2)$$

Where $\dot{Q}_{t=defrost}$ is the heating capacity, in kW, at the end of the working cycle and just before initiating the defrost process, and $\dot{Q}_{t=0}$ is the

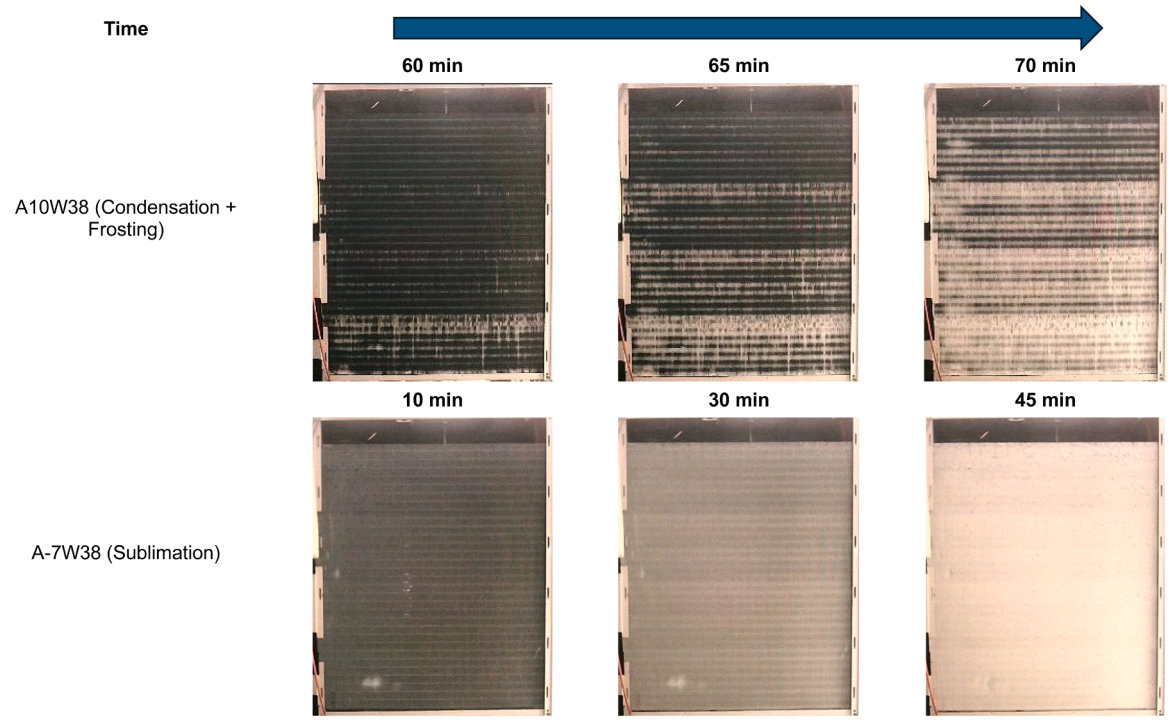

Fig. 4. Frost formation photos under working conditions A10W38 and A-7W38 (fixed RH=90 %).

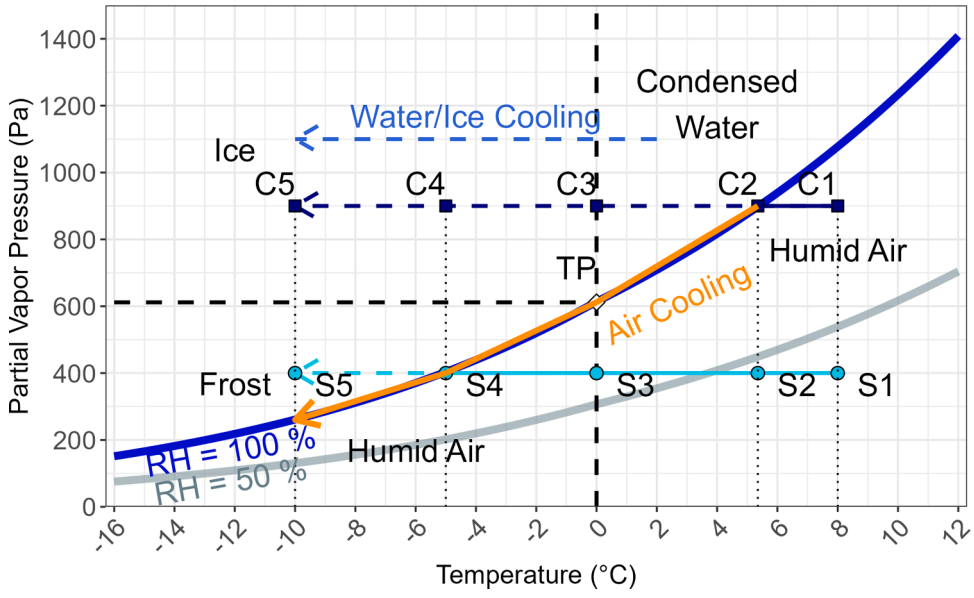

Fig. 5. Phase diagram of water vapor in the air.

heating capacity at the beginning of the working cycle, and without any frost formation or condensed water on the evaporator's surface.

Table 3 shows that there is an uncertainty in the determination of the beginning of the defrost cycle by ±3 % based on the capacity degradation factor (the set point should be 15 %). The points with an air dry-bulb temperature of 10 and 7°C have values for the partial pressure higher than the triple-point. Therefore, the FTHX operates first in dehumidification conditions for an extended period without frost generation (1 hour in A10, and 30 minutes in A7), as shown in Fig. 6. Subsequently, once the frost generation process starts, freezing occurs first in the lower circuits due to a large amount of drained condensate, and then it occurs in the intermediate and upper circuits. This frost growth process is fast, obtaining short frost formation periods and with values for the BR below 100 % due to the uniformity of frost growth.

It is very relevant to see that when C+F typology occurs, low values of BR introduce a higher heat pump capacity degradation. The explanation for that is associated with the fact that when the water is frozen, it is converted directly to ice, with a higher density than frost, and it blocks a total part of the heat exchanger, preventing the air flow and degrading the heat transfer on that part. As the pressure in all the circuits is the same, if the evaporating pressure decreases in one of the circuits, it will affect all of them, and the effect on the system performance will be high, even if the air flows properly in some zones of the FTHX.

Based on that observation, a good design practice to improve the

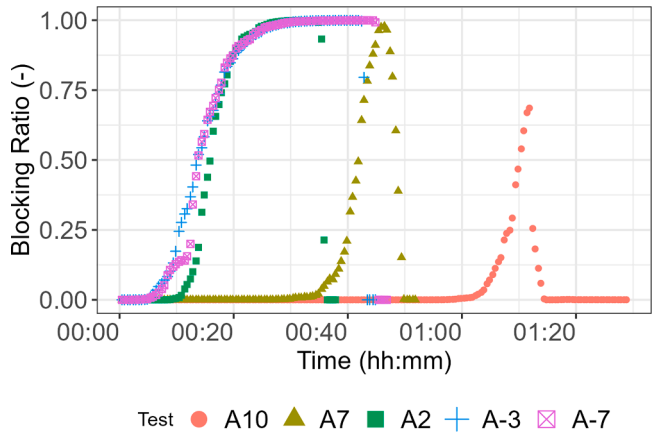

Fig. 6. Blockage ratio (BR) as a function of time for five test points.

Table 3
Summary of experimental results for the characterization of frost formation mechanism.

Variable	A10	A7	A2	A-3	A-7
HCD (%)	17.7	17.1	14.7	12.9	16.4
Partial pressure of water vapor (Pa)	1071	851	608	416	316
Frost mechanism*	C+F	C+F	S	S	S
BR (%)	70	97	100	100	100

* C+F=Condensation + frost; S=Sublimation.

FTHX performance under these conditions is to redesign the refrigerant circuits to allow the circuits with higher refrigerant temperature (ex., superheating zone) to pass at the bottom of the heat exchanger to mitigate the conversion of condensed water to high-density ice with time. This phenomenon also indicates that using the air pressure drop or air flow as an indicator for initiating a defrost could introduce important degradations in the COP of the system.

On the other hand, the values obtained for the partial pressure at the points with an air temperature of 2, -3, and -7 °C are lower than the partial pressure at the triple-point. In this case, the FTHX operates in sublimation frosting conditions, where the moisture in the air freezes directly in contact with the evaporator's low-temperature surface. So, it results in homogeneous frost growth at the FTHX surface. Moreover, under these conditions, we can observe in Fig. 6 that frost formation starts from the beginning, unlike the A10 and A7 points (9 minutes in A2, and 4 minutes in A-3 and A-7).

Observing the general trend, we can conclude that, at negative temperatures and low moisture content, the frost generation process penalizes the performance of the unit due to a slow growth process and a higher number of defrost cycles. In these conditions, the frost is formed by a sublimation mechanism. On the other hand, at moderate temperatures, despite the high humidity content in the air, the C+F process allows longer operating times with only condensation and a flow area free of frost for longer time but when ice begins to be formed at the bottom of the heat exchanger and as a consequence of it higher density a fast degradation stars. This fast degradation process is a consequence of the maldistribution of frost formation, which introduces a higher and faster penalty on the system's performance. In the following subsection, the frost formation by sublimation will be analyzed in more detail.

3.2. Analysis of the frost formation process by sublimation

The current experimental study focuses on determining the relationship between frost formation, evaporation temperature, and dew and wet-bulb air temperatures. In that way, a scale that evaluates the severity of the frosting process on the performance of AWHP could be determined.

Table 4 shows the working time before the defrost cycle is activated by the system, the collected amount of water after the defrost cycle, and the estimation of retained water within the FTHX. Some tests were repeated to evaluate the intrinsic process variability. The retained water, on average, is nearly 4 % of the total water collected, but in the coldest conditions, this percentage could increase up to 12 %.

It is worth mentioning that if the blowing process is not performed after the defrost process to remove the remaining water when the unit finishes the defrost cycle, a heavy mist can be observed around the FTHX caused by the evaporation of the retained water between fins. In the current work, no methodology has been implemented to estimate the amount of water evaporated due to this phenomenon, but we deem it necessary to record this fact. This mist is visible in situ and monitored by humidity sensors that reach near-saturation values within 10 minutes of defrosting.

Also, Table 4 shows that the highest amount of condensed water takes place for tests with RH values of the highest ambient temperatures; this is related to the fact that each test has a different duration, as the capacity degradation defines them. Once the time is considered, an average value of how much water is frosted/condensed on the heat exchanger per minute (water deposition rate) is obtained. Fig. 7 (a) represents the water deposition rate as a function of air temperature. It shows that there is a higher deposition rate as the evaporating temperature increases for a constant relative humidity. These results also show that the amount of frost in the heat exchanger is not the only factor to consider in order to evaluate the degradation of the system. In fact, tests at RH=90 % show a higher frost deposition than at 80 %, and probably with a different structure in the heat exchanger that speeds up the degradation of the performance. In addition, it should be pointed out that when air temperature is below 0 °C, the phase change of water vapor is produced directly by sublimation, but for air temperatures higher than 0 °C, both sublimation and C+F formation can be produced even if the temperature of the tube is lower than 0 °C.

Fig. 7 (b) shows the relation between the mean water deposition rate and the difference between the evaporating temperature and the air dew-point temperature, and for that situation, it can be seen that the mean water deposition rate is properly reproduced by a straight line.

Fig. 8 represents the duration of the frost formation period before the defrost starts as a function of air temperature. It shows that the frost formation period is almost the same for all the tests performed at RH=90 %, but for the tests performed at RH=80 %, the duration of the frost formation period increases as the evaporation temperature is reduced. This finding also points to the previous statement that indicates that, depending on the relative humidity, a different frost morphology could be observed in the FTHX, as it depends on the degree of air

Table 4
FTHX condition and the amount of water collected after the defrosting cycle.

Air condition (T_{db} (°C), RH (%))	Working Time (min)	Frost Mechanism (-)	Collected water (g)	Retained water (g)
(7,65)	278.25	C+F	4488	143
(5,65)	231.33	S	4115	143
(5,80)	131.67	C+F	4036	179
(2, 80)	153	S	3631	155
(0, 80)	120.17	S	2870	196
(-3, 80)	211.83	S	3738	167
(-5,80)	246.83	S	3661	128
(-7,80)	206	S	2640	73
(-12,80)	253	S	2005	321
(5,90)	125.33	C+F	4407	191
(2,90)	102.5	C+F	2668	158
(0,90)	77	S	2424	124
(-3,90)	93.83	S	2536	61
(-5,90)	111	S	2290	111
(-7,90)	94	S	1804	130
(-12,90)	107	S	1705	354

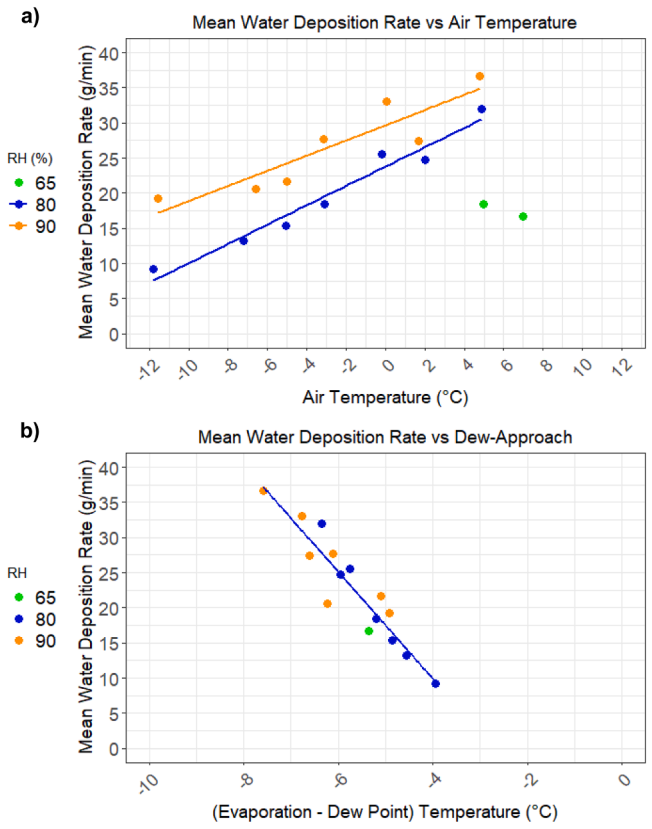

Fig. 7. Water deposition rate under different RH values as a function of a) air temperature; and b) the difference between the evaporating temperature and the air dew-point temperature.

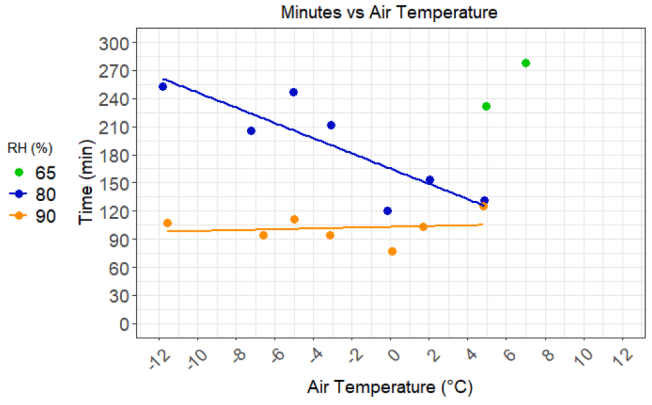

Fig. 8. Operating period until defrost start versus air temperature under different RH values.

supersaturation. In that sense, the frost layer could be formed by hollow or solid tubes. Also, the frost formation period is similar for the same air dry-bulb temperature in RH=90 % tests, while the differences are higher for the ones with RH=80 %. This could show us that frost formation depends more on the air temperature when the relative humidity is low. The operation time until the heat pump performs a defrost cycle tends to be shorter as the air temperature increases.

Fig. 9 plots the evaporating temperature and air-side pressure drop as a function of time for the different tests. The points with higher relative humidity require lower times to initiate the defrost process. The evolution of the evaporating temperature shows an almost linear degradation of the system's performance up to a specific time, where the degradation accelerates significantly. The evolution of the evaporating temperature also shows that usually the defrost starts when the evaporating temperature has decreased approximately by 5 K.

Regarding the behavior of the pressure drop, the defrost process usually initiates between 20 and 30 Pa. This fact probably points to different profiles/characteristics in the morphology of the frost in the heat exchanger, depending on the conditions. In addition, another characteristic shown by the Fig.s is that the pressure drop increases following a given trend, but some minutes before the defrost, the pressure drop is reduced to increase more significantly afterwards. This process could be interpreted in terms of the observations reported by Guo et al. (2008) regarding the different processes involved in frost formation. First, the ice crystals formed on the surface of the heat exchanger increase the surface roughness, which results in improved heat transfer (increased heat exchange surface area) and an increase in the pressure drop. Once the frost accumulation increases, two negative effects appear: an increase in thermal resistance and a reduction in the free passage area for air. Nevertheless, from the observed results, the pressure drop and, consequently, the airflow reduction seem to be the most important factors in the performance degradation. This degradation becomes severe at the end of the frosting period, when the air pressure drop also becomes higher. This could be related to the densification process of the frost layer that gradually reduces the porosity and increases the frost density with time. This gradually reduces the ability of air to penetrate through the frost layer. Just before the defrosting cycle, the frost density will be near the density of ice, and its porosity is almost zero. This results in a severe reduction in air flow rate through the evaporator, which could explain this exponential increase in the air-side pressure drop just before starting the defrost cycle.

From these observations, a conclusion related to the different alternatives to initiating a defrost process could be suggested. A good defrost criterion should be based on the refrigerant-side to quantify the degradation of the AWHP performance due to frost formation. Any other criteria that are based on the air-side could underestimate or overestimate the defrost timing due to the high variability of physical factors that affect frost morphology and behavior.

Considering those comments and the fact that the criterion used for defrosting depends on the capacity degradation, a reformulation of it based only on the evaporation temperature can be given according to the expression shown in Equation 3:

$$\rho\left(P\left(T_{edf}\right),\ T_{edf}+SH\right)\cdot\epsilon_v\left(\frac{P_c}{P\left(T_{edf}\right)}\right)\ =0.85\cdot\rho\left(P\left(T_e\right),\ T_e+SH\right)\cdot\epsilon_v\left(\frac{P_c}{P\left(T_e\right)}\right) \tag{3}$$

Where T_{edf} is the evaporation temperature at which the defrost process starts. T_e is the evaporation temperature after a defrost process is finished. ϵ_v is the compressor volumetric efficiency. P_c is the condensing pressure. SH is the superheat. Finally, ρ is the density of refrigerant on the given working conditions. That expression assumes that the enthalpy difference in the evaporator and the condensation temperature do not depend significantly on the evaporation temperature.

We have emphasized the evaporation temperature because it is an easy parameter to measure in commercial heat pumps. In fact, the continuous measurement of evaporation temperature is already included in many commercial AWHPs as a standard and easy indicator of the system's performance. Besides, it is the most relevant variable to the frost formation process. The increase of frost layer thickness and density results in a degradation of air flow rate and, subsequently, the evaporation temperature.

It is worth mentioning that other variables, such as flow rate (it is very difficult to measure in real installations), enthalpy change (does not change significantly with evaporation temperature), or pressure drop on the refrigerant-side (it is expensive to determine but also does not have a significant impact on frost formation), will complicate the study further without adding significant value.

Based on those assumptions, and knowing the compressor

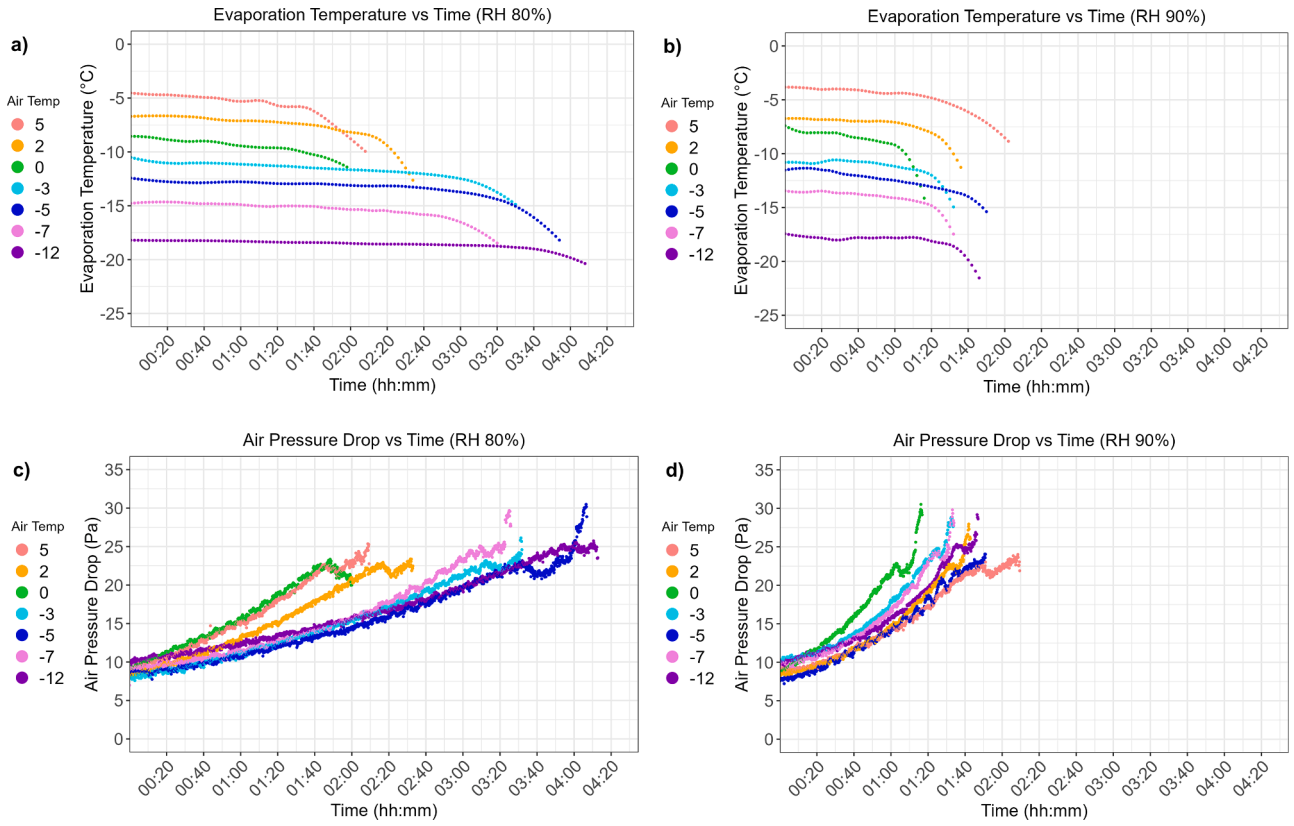

Fig. 9. Evaporation temperature versus time for a) RH=80 %, and b) RH=90 %; and air-side pressure drop vs. time for c) RH=80 %, and d) RH=90 %.

characterization curves, for a given operation point, it is possible to determine the evaporation temperature at which the defrost must be initiated from the value of the condensing and evaporating temperatures after a defrost cycle (at the beginning of the frost formation phase).

4. Conclusions

In this paper, an analysis of the frost formation process in FTHX in a commercial AWHP working under real operating conditions is implemented. These conditions result in different frost formation mechanisms and morphologies. The criterion used to initiate the defrost was to have a degradation of 15 % in the heating capacity. The results have been analyzed in terms of blockage ratio, evaporating temperature, air-side pressure drop, and amount of water condensed after the defrosting. The conclusions of this analysis are as follows.

The evaluation of frost formation and growth in different working conditions shows that the blockage ratio or the amount of water collected is not enough to evaluate the real degradation of the heat pump's performance because of the frost. Other parameters like the frost structure or the frost distribution could also have a significant relevance to that process.

Regarding the tests in which the frost was formed due to sublimation, the following observations are summarized:

- The amount of frost in the heat exchanger is not a good indicator for defining heat pump degradation.
- A constant mean frost deposition rate was detected as a function of the relative humidity.
- Regarding the time at which the defrost cycle starts, there was no time dependence on the air temperature for the conditions when the air is in almost saturated conditions.
- The air-side pressure drop values increase following a clear trend with time up to a certain point, at which it begins to decrease for a few minutes. After that period, there is a stage of rapid increase of the pressure drop, which activates the defrost cycle. The observation could be related to the densification process of the frost layer. Its density increases while its porosity decreases with time till reaching the ice density and zero porosity. That accelerates the degradation as it results in higher blockage to the air flow.

From all the observations of this experimental campaign, it has been shown that the impact of the evaporators that work under frost conditions on the heat pump performance is very complex, and it is difficult to analyze in terms of the air-side variables. In fact, properties like frost structure or non-uniform frost distribution seem to be more determinant in the degradation of the heat pump performance than pressure drop or the amount of frost. Therefore, from a practical point of view, the parameters that are probably the most suitable for the defrosting decision would probably be related to internal (refrigerant-side) parameters. In this context, a proposed criterion to estimate the onset of the defrost process was derived based on the evolution of the evaporation temperature, which is an easy parameter to measure, as it reflects clearly the impact of the frost formation on the degradation of an AWHP's performance.

Based on the obtained results, a future evaluation of the possible influence of the coating on the frost formation process will be done, as some works in literature have reported the advantages of some surface treatment techniques that are adopted to delay the initiation of the defrost process. Most of these studies, for instance Wang et al. (2015b) and Boyina et al. (2019), analyze this process only for one type of frost formation process, or focus on the external characteristics of the frost, which may not be enough to determine the real degradation of the heat pump performance under frost conditions.

CRediT authorship contribution statement

David Alarcón-Gallén: Writing – original draft, Validation, Investigation, Formal analysis, Data curation. **Javier Marchante-Avellaneda:** Writing – original draft, Validation, Investigation, Formal analysis, Data curation. **Abdelrahman H. Hassan:** Writing – review & editing, Visualization, Validation, Supervision, Project administration, Methodology, Investigation. **Emilio Navarro-Peris:** Writing – review & editing, Visualization, Validation, Supervision, Resources, Project administration, Methodology, Investigation, Funding acquisition, Conceptualization.

Declaration of competing interest

The authors declare that they have no known competing financial interests or personal relationships that could have appeared to influence the work reported in this paper.

Acknowledgements

This work has been funded by the project "*Investigación en la próxima generación de bombas de calor aerotérmicas para edificios integradas en los sistemas de calefacción/refrigeración y agua caliente sanitaria*", Ref. PID2023-148964OB-I00, by the Spanish Ministry of Science, Innovation and Universities. The authors are grateful for the support given.

Marchante-Avellaneda J. would like to acknowledge the Universitat Politècnica de València (UPV) for the grants for contracts for research personnel access (Ref. PAID-10-23); and initial research projects (Ref. PAID-06-24).

References

Boyina, K.S., Mahvi, A.J., Chavan, S., Park, D., Kumar, K., Lira, M., Yu, Y., Gunay, A.A., Wang, X., Miljkovic, N., 2019. Condensation frosting on meter-scale superhydrophobic and superhydrophilic heat exchangers. Int. J. Heat. Mass Transf. 145, 118694. https://doi.org/10.1016/J.IJHEATMASSTRANSFER.2019.118694.

Da Silva, D.L., Hermes, C.J.L., Melo, C., 2011. Experimental study of frost accumulation on fan-supplied tube-fin evaporators. Appl. Therm. Eng. 31, 1013–1020. https://doi.org/10.1016/J.APPLTHERMALENG.2010.11.006.

da Silva, D.L., Melo, C., Hermes, C.J.L., 2017. Effect of frost morphology on the thermal-hydraulic performance of fan-supplied tube-fin evaporators. Appl. Therm. Eng. 111, 1060–1068. https://doi.org/10.1016/J.APPLTHERMALENG.2016.09.165.

European Commission, n.d. Heat pumps [WWW Document]. URL https://energy.ec.europa.eu/topics/energy-efficiency/heat-pumps_en (accessed 3.6.25).

FFmpeg Developers, 2016. ffmpeg tool (Version be1d324).

Guo, X.M., Chen, Y.G., Wang, W.H., Chen, C.Z., 2008. Experimental study on frost growth and dynamic performance of air source heat pump system. Appl. Therm. Eng. 28, 2267–2278. https://doi.org/10.1016/J.APPLTHERMALENG.2008.01.007.

Hwang, J., Cho, K., 2014. Numerical prediction of frost properties and performance of fin–tube heat exchanger with plain fin under frosting. Int. J. Refrig. 46, 59–68. https://doi.org/10.1016/J.IJREFRIG.2014.04.026.

Liang, S., Wang, H., Gao, X., Tian, X., Zhu, H., Hu, S., Lin, C., 2024. Experimental study on the operating performance of the air source heat pump (ASHP) with variable outdoor airflow rate under the standard frosting condition. Energy Built Environ. 5, 719–726. https://doi.org/10.1016/J.ENBENV.2023.06.001.

R Foundation for Statistical Computing, V.Austria., 2021. R: a language and environment for statistical computing [WWW Document]. URL https://www.r-project.org/ (accessed 7.21.25).

Song, M., Dang, C., 2018. Review on the measurement and calculation of frost characteristics. Int. J. Heat. Mass Transf. 124, 586–614. https://doi.org/10.1016/J.IJHEATMASSTRANSFER.2018.03.094.

Song, M., Deng, S., Dang, C., Mao, N., Wang, Z., 2018. Review on improvement for air source heat pump units during frosting and defrosting. Appl. Energy 211, 1150–1170. https://doi.org/10.1016/J.APENERGY.2017.12.022.

Tang, R., Wang, F., Wang, Z., Yang, W., 2021. Division of frosting type and frosting degree of the air source heat pump for heating in China. Front. Energy Res. 9. https://doi.org/10.3389/fenrg.2021.708478.

Wang, F., Liang, C., Yang, M., Fan, C., Zhang, X., 2015a. Effects of surface characteristic on frosting and defrosting behaviors of fin-tube heat exchangers. Appl. Therm. Eng. 75, 1126–1132. https://doi.org/10.1016/J.APPLTHERMALENG.2014.10.090.

Wang, F., Liang, C., Yang, M., Zhang, X., 2015b. Effects of surface characteristics on liquid behaviors on fin surfaces during frosting and defrosting processes. Exp. Therm. Fluid. Sci. 61, 113–120. https://doi.org/10.1016/J.EXPTHERMFLUSCI.2014.10.022.

Yoo, J.W., Chung, Y., Kim, G.T., Song, C.W., Yoon, P.H., Sa, Y.C., Kim, M.S., 2018. Determination of defrosting start time in an air-to-air heat pump system by frost volume calculation method. Int. J. Refrig. 96, 169–178. https://doi.org/10.1016/J.IJREFRIG.2018.08.014.

Zhang, L., Jiang, Y., Dong, J., Yao, Y., Deng, S., 2019. An experimental study on the effects of frosting conditions on frost distribution and growth on finned tube heat exchangers. Int. J. Heat. Mass Transf. 128, 748–761. https://doi.org/10.1016/J.IJHEATMASSTRANSFER.2018.09.016.

Zhang, L., Song, M., Deng, S., Shen, J., Dang, C., 2022. Frosting mechanism and behaviors on surfaces with simple geometries: a state-of-the-art literature review. Appl. Therm. Eng. 215, 118984. https://doi.org/10.1016/J.APPLTHERMALENG.2022.118984.

Zhu, J.H., Sun, Y.Y., Wang, W., Deng, S.M., Ge, Y.J., Li, L.T., 2015. Developing a new frosting map to guide defrosting control for air-source heat pump units. Appl. Therm. Eng. 90, 782–791. https://doi.org/10.1016/J.APPLTHERMALENG.2015.06.076.